The Rotational Zeeman Effect of Carbonylselenide, OCSe, its Molecular Electric Quadrupole Moment, and the Effects of the C=Se Stretching and the Bending Vibration; A High Resolution Microwave Fourier Transform Study

Armin Klesing and Dieter H. Sutter

Institut für Physikalische Chemie der Christian-Albrechts-Universität Kiel, Ludewig-Meyn-Straße 8, D-24098 Kiel, Germany

Z. Naturforsch. **48a**, 968–986 (1993); received July 17, 1993

The results of a high resolution microwave Fourier transform study of the rotational Zeeman effect in the $J' = 2 \rightarrow J'' = 1$ transitions of $^{16}O^{12}C^{80}Se$, $^{16}O^{12}C^{78}Se$, and $^{16}O^{12}C^{77}Se$ are reported. From the observed g-values and susceptibility anisotropies, experimental values were derived for the molecular electric quadrupole moment, for the anisotropy in the second moments of the electronic charge distribution, for the paramagnetic susceptibility perpendicular to the OCSe chain, and for the sign of the electric dipole moment. From the Zeeman data observed for the l-type doublet, the paramagnetic susceptibility parallel to the OCSe-axis, which by symmetry is zero for the linear configuration, could be derived as a function of the bending angle, β. Ab initio calculations of the molecular electric quadrupole moment were carried out. Fair agreement with the experimental value was obtained at the CID/LANLIDZ+pol level of computation.

The Lorentz-Stark effect, which usually leads to perturbations in the Zeeman patterns of l-type doublet lines, vanishes if data collection starts with a delay 2 μs after the end of the exciting pulses. This finding is attributed to the short collisional lifetime of fast molecules and suggests new experiments in the field of rotational relaxation studies.

1. Introduction

In rotational Zeeman studies of stiff molecules in their vibronic ground state the splitting of the rotational transitions by the first and second order magnetic field effects directly leads, respectively, to the experimental determination of the molecular g-values and the anisotropies in the molecular magnetic susceptibility tensor. Combination of the measured g-values and magnetic susceptibility anisotropies then leads to the principal inertial axes components of the molecular electric quadrupole moment tensor, i.e. to molecular quantities, which are of great interest for the calculation of short range intermolecular forces. Furthermore, accurately measured g-values of two isotopic species give information on the orientation of the electric dipole moment within the molecule.

In excited vibrational states intramolecular motion may lead to additional magnetic moments. Typical examples are the magnetic moment associated with low barrier internal rotation of methyl tops [1] and with degenerate vibrations in symmetric tops and linear molecules such as OCSe studied here [2–5].

In the following we present the results of a high resolution rotational Zeeman effect study of the ^{80}Se, ^{78}Se, and ^{77}Se isotopomers of carbonylselenide in their vibronic ground state. For the most abundant species, $^{16}O^{12}C^{80}Se$, we also report results obtained for molecules in their first excited state of the C=Se stretching or the bending vibration, respectively. This work complements and extends an early investigation by Shoemaker and Flygare [6], which was confined to the vibronic ground state. With the accuracy of the frequency determinations improved by more than an order of magnitude, the determination of the orientation of the electric dipole moment is now unambiguous and the uncertainties in the experimental value for the molecular electric quadrupole moment could be reduced to 0.02 DÅ.

2. Experimental

The sample – all isotopes in natural abundance – was prepared by Prof. Dr. H. Willner, Hannover. It was kindly provided by Dr. J. Demaison after comple-

Reprint requests to Prof. Dr. D. H. Sutter, Institut für Physikalische Chemie, Universität Kiel, Olshausenstraße 40, D-24098 Kiel, Germany.

0932-0784 / 93 / 1000-0968 $ 01.30/0. – Please order a reprint rather than making your own copy.

tion of a careful study of its mm-wave spectrum [7].

In view of its limited stability the sample was stored in a glas bulb, cooled by liquid nitrogen. For the measurements the sample was allowed to warm up gently until its vapour pressure reached about 10 mTorr for filling the brass waveguide absorption cell. The latter was kept at a temperature of about −65 °C by methanol flowing through a cooling jacket. Before sealing the cell for spectroscopy, the sample pressure was pumped down to approximately 1 mTorr. Under these conditions the sample proved sufficiently stable to allow for spectroscopy sessions of up to one hour without the necessity of refilling the absorption cell.

The Zeeman spectra were recorded by means of waveguide microwave Fourier transform spectroscopy. As compared to our original set-up described in [8], the signal oscillator frequency was derived from the local oscillator by pulsed single side band modulation. This not only simplifies the set-up, but also eliminates problems arising from signal oscillator leakage into the detection system during data collection. A detailed description of the system will be given in a forthcoming publication in this Journal.

Within a microwave Fourier transform spectrometer [9, 10] the molecules are exposed to a short (~50 nsec in the present investigation) intense (~5 W) microwave pulse. This pulse coherently drives those molecules, for which the carrier frequency in the pulse is near resonant to a dipole allowed transition, into a corresponding intermediate (non-eigen) state. In the following we will refer to this subensemble of molecules as the *absorbers*. After the pulse the absorber molecules are left with a non-stationary probability density distribution, which wobbles at the resonance frequency corresponding to the energy difference of the upper and lower eigenstate previously mixed by the short intense pulse. This wobbling leads to a faint molecular emission signal which propagates in the same direction as the exciting pulse. It decays mainly due to collisions and Doppler dephasing. (In comparison radiational damping due to the energy loss associated with the coherent emission at the resonance frequency is negligible). The faint molecular signal is first amplified by a high gain low noise microwave amplifier. For digitization it is then heterodyned against a local oscillator. In our set-up the local oscillator frequency is exactly 30 MHz below the carrier frequency of the exciting pulse. This leads to a down-conversion of the molecular emission signals into a

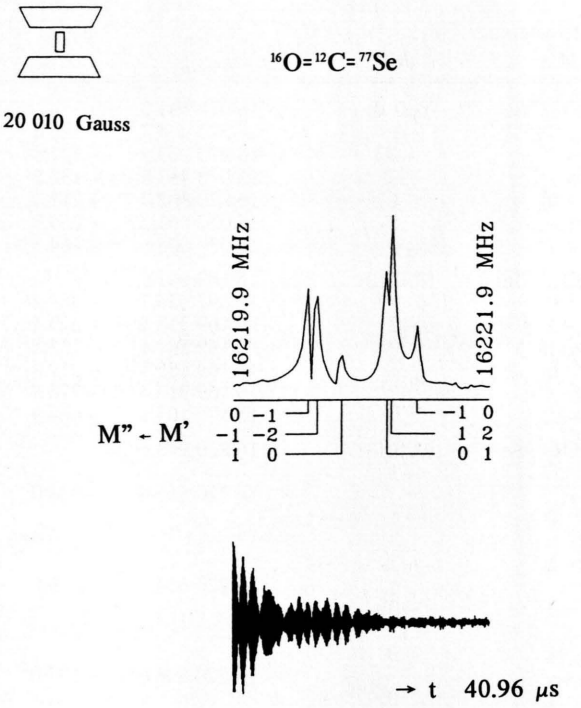

Fig. 1. Amplitude FT-spectrum and transient emission signal of the $J'=2 \rightarrow J''=1$ rotational transition of $^{16}O^{12}C=^{77}Se$ in its vibronic ground state in a magnetic field of 2.0010 Tesla. With the electric vector of the incident microwave radiation perpendicular to the magnetic field the $\Delta M = \pm 1$ selection rules applies (compare insert). The transient emission signal shown here results from a down conversion of the original microwave signal into the 30 MHz region. For noise reduction $1.3 \cdot 10^7$ transient emissions were sampled at a sampling interval of 10 ns. A sequence of 4096 data points, corresponding to an observed decay time of 40.96 μs was taken for each emission. The final determination of the satellite frequencies was carried out by a direct least squares fit (see text).

frequency band around 30 MHz. These intermediate frequency signals are then rapidly digitized at 10 nsec intervals.

In the present investigation typically strings of 2 K or 4 K data points were sampled after each pulse, and the signal sequencies of 10^4 to 10^7 transient decays were averaged up for noise reduction.

Combined with the known local oscillator frequency, the observed frequency of the transient emission signal directly gives the molecular resonance frequency, and the observed decay time corresponds to the line width, which would be observed in frequency domain spectroscopy. If several resonances are hit by the exciting pulse, a beat signal results, which allows for the reconstruction of the corresponding molecular emission frequencies and intensities. There are different

Isotopomer M''	(v_1, v_2, v_3) M'	M_I	$\nu_{0,\mathrm{exp}}$ $\nu_{H,\mathrm{exp}}$	$\Delta\nu_{\mathrm{exp}}$	$\Delta\nu_{\mathrm{calc}}$	$\delta\nu$	Rel. Int. %
$OC^{80}Se$	(0, 0, 0)		16 070 591.3				
0	−1		16 070 204.7	−386.6	−386.2	−0.4	50.0
−1	−2		16 070 263.5	−327.8	−328.0	+0.3	100.0
1	0		16 070 457.8	−133.5	−133.8	+0.3	16.5
0	1		16 070 802.7	+211.4	+211.5	−0.1	50.0
1	2		16 070 861.2	+269.9	+269.7	+0.2	100.0
−1	0		16 070 005.6	+464.3	+463.9	+0.4	16.5
$OC^{78}Se$	(0, 0, 0)		16 169 642.9				
0	−1		16 692 255.7	−387.2	−387.2	+0.3	50.0
−1	−2		16 169 313.5	−329.4	−329.3	−0.1	100.0
1	0		16 169 507.4	−135.5	−135.1	−0.4	16.5
0	1		16 169 855.8	+212.9	+212.8	+0.1	50.0
1	2		16 169 913.4	+270.5	+271.0	−0.5	100.0
−1	0		16 170 107.8	+464.9	+465.2	−0.3	165.5
$OC^{77}Se$	(0, 0, 0)		16 220 943.6				
0	−1	$-\frac{1}{2}$			−386.0		50.0
			16 220 555.6	−388.0		0.3	
0	−1	$+\frac{1}{2}$			−390.6		50.0
−1	−2	$-\frac{1}{2}$			−327.7		100.0
			16 220 614.0	−329.6		+0.4	
−1	−2	$+\frac{1}{2}$			−332.3		100.0
1	0	$-\frac{1}{2}$			−137.9		16.5
			16 220 806.6	−137.0		−1.4	
1	0	$+\frac{1}{2}$			−133.3		16.5
0	1	$-\frac{1}{2}$			+211.1		50.0
			16 221 156.7	+213.1		−0.3	
0	1	$+\frac{1}{2}$			+215.7		50.0
1	2	$-\frac{1}{2}$			+269.4		100.0
			16 221 215.1	+271.5		−0.2	
1	2	$+\frac{1}{2}$			+274.0		100.0
−1	0	$-\frac{1}{2}$			+468.4		16.5
			16 221 409.9	+466.3		+0.2	
−1	0	$+\frac{1}{2}$			+463.8		16.5
$OC^{80}Se$	(0, 0, 1)		16 017 540.3				
0	−1		16 017 152.6	−387.7	−386.5	−1.2	50.0
−1	−2		16 017 211.5	−328.8	−328.4	−0.4	100.0
+1	0		16 017 405.2	−135.1	−134.7	−0.4	16.5
0	+1		16 017 752.4	+212.1	+212.2	−0.1	50.0
+1	+2		16 017 810.9	+270.6	+270.3	+0.3	100.0
−1	0		16 018 004.6	+464.3	+464.0	+0.3	16.5

Table 1. Zeeman multiplets of the $J' = 2 \rightarrow J'' = 1$ rotational transitions of $^{16}O^{12}C^{80}Se$, $^{16}O^{12}C^{78}Se$, and $^{16}O^{12}C^{77}Se$ in the vibronic ground state, and of $^{16}O^{12}C^{80}Se$ in the first excited state of the C=Se stretching vibration ($\bar{\nu} = 643.5\ \mathrm{cm}^{-1}$), all observed in a magnetic field of 20010(5) Gauss = 2.0010(5) Tesla. M'' and M' denote the M-values of the lower and upper state respectively. M_I denotes the magnetic quantum number of the nuclear spin of the ^{77}Se nucleus. At a field of 2 Tesla it is effectively uncoupled from the overall rotation and the selection rule $\Delta M_I = 0$ applies. However, spin-rotation coupling still leads to a small splitting of the $M_I = \pm\frac{1}{2}$ states. Its effect was calculated from the observed spin-rotation coupling constant $C_{N,^{77}Se} = 4.60(1)$ kHz [16] and the nuclear g-value $g_{I,^{77}Se} = 0.534$ (Appendix E in [24]). ν_0 denotes the zero field frequencies. All frequencies are given in kHz.

numerical methods to extract the molecular resonance frequencies, intensities, and decay times from the measured raw data. In our case a two step procedure was used. It consists of a standard discrete Fourier transform analysis, followed by an iterative direct least squares fit of the frequencies, intensities and relaxation times to the observed data points. In other words, the Fourier transform analysis merely provides the initial values for the subsequent iterative least squares procedure. Especially in the case of narrow multiplets, such as are typically encountered in rotational Zeeman effect studies, the least squares procedure leads to much more reliable spectral data than the Fourier transform analysis [11]. A computer program developed by Haeckel and Mäder and described in [12] was used for this purpose. Our Zeeman multiplet frequencies obtained this way are compiled in Table 1. In Figure 1 we present a typical Fourier transform amplitude spectrum obtained in the present investigation.

3. Analysis of the Zeeman Multiplets in the Vibronic Ground State and in the First Excited State of the C=Se Stretching Vibration

For the analysis of the Zeeman multiplets in the vibronic ground state and in the first excited state of the C–Se stretching vibration at 643.5 cm^{-1} [13] we have used the standard energy expression for a linear molecule (cf. Chapt. III.D in [14]). Within this approach the first and second order contributions due to the magnetic field are given by the following effective energy expression:

$$\langle J, M | H_{\text{eff}} | J, M \rangle = -\mu_N H_Z M g_\perp - \frac{1}{2N_A} \xi_{\text{bulk}} H_Z^2 + \frac{H_Z^2}{N_A} \frac{3M^2 - J(J+1)}{3(2J-1)(2J+3)} (\xi_\parallel - \xi_\perp). \quad (1)$$

Here μ_N is the nuclear magneton. H_Z is the magnetic field (assumed to point in the direction of the laboratory frame Z-axis). M is the quantum number for the Z-component of the rotational angular momentum. $\xi_{\text{bulk}} = (\xi_{aa} + \xi_{bb} + \xi_{cc})/3$ is the so-called bulk susceptibility. $\xi_\parallel = \xi_{aa}$ is the component of the susceptibility tensor parallel to the internuclear axis. $\xi_\perp = \xi_{bb} = \xi_{cc}$ is the component of the susceptibility tensor perpendicular to the nuclear chain. N_A is Avogadros number. We assume that the theoretical expressions for the effective $g_\perp$-value and for the susceptibilities are approximately given by the vibrational ground state expectation values of the corresponding rigid rotor expressions [15].

For the ^{77}Se-species we note that spin-rotation coupling of the ^{77}Se nucleus should be accounted for in principle. It causes each Zeeman satellite to split symmetrically into a narrowly spaced doublet corresponding to the $M_{I_{Se}} = \frac{1}{2}$ and $M_{I_{Se}} = -\frac{1}{2}$ states, respectively. However this splitting was calculated to be less than 5 kHz [16], i.e. well below the resolution in our waveguide spectrometer. Since the spin-rotation splitting leaves the intensity weighted mean frequency of each M-satellite doublet unchanged, we have neglected it right from the outset.

The $g_\perp$-values and susceptibility anisotropies, $(\xi_\parallel - \xi_\perp)$, which resulted from a least squares fit to the experimental splittings reported in Table 1 are given in Table 2. Also given are the rotational constants (calculated as $B_\perp = \frac{1}{4}\nu_{(2\to1)}$ and the second moments of the nuclear charge distribution, $\sum Z_n a_n^2$. The latter were calculated from the isotopic masses and from the microwave r_e-structure, $r_{e(O=C)} = 1.1534$ Å, $r_{e(C=Se)} = 1.7098$ Å [17]. For comparison we also quote ab initio values for the individual components of the magnetic susceptibility tensor as calculated recently by U. Fleischer (private communication). For his calculation he used the IGLO-method with the following basis: 20s14p11d3f/11s7p2d (fully localized IGLO). The anisotropy in the susceptibilities, i.e. $(\xi_\parallel - \xi_\perp)_{\text{IGLO}}$ calculated from his results for the individual components: $\xi_\perp = -42.9 \cdot 10^{-6}$ erg G^{-2} mol^{-1}, $\xi_\parallel = -52.2 \cdot 10^{-6}$ erg G^{-2} mol^{-1}, deviates much less from the experimental data than in the case of the theoretically much more demanding molecule OCCCS. For references to the IGLO-method we refer to our joint publication on the rotational Zeeman effect in OCCCS [18].

	$OC^{80}Se$	$OC^{78}Se$	$OC^{77}Se$	$OC^{80}Se$ $v_3=1$
B/MHz	4017.65062(46)	4042.41728(31)	4055.24323(24)	4004.39295(34)
$g_\perp$	−0.019592(8)	−0.019679(8)	−0.019723(13)	−0.019625(10)
$\xi_\parallel - \xi_\perp$	−10.159(12)	−10.159(12)	−10.170(19)	−10.136(15)
$\xi_\perp^{(p)}$	267.01(51)	266.65(52)	266.47(52)	–
$\sum_{n=1}^{\text{nuclei}} Z_n a_n^2$	60.49(12)	60.41(12)	60.37(12)	–
$Q_\parallel$	−0.253(18)	−0.233(18)	−0.209(29)	−0.337(23)
$\left\langle \sum_j^{\text{electr}} (b_j^2 - a_j^2) \right\rangle$	−60.54(12)	−60.46(12)	−60.41(12)	–

Table 2. Rotational constants, g-values, susceptibility anisotropies, paramagnetic susceptibilities perpendicular to the linear chain, second moments of the nuclear charge distribution, molecular electric quadrupole moments, and asymmetry in the second moments of the electron charge distribution for $^{16}O=^{12}C=^{80}Se$, $^{16}O=^{12}C=^{78}Se$, $^{16}O=^{12}C=^{77}Se$, and for $^{16}O=^{12}C=^{80}Se$ also in the first excited state of the C=Se stretching vibration. The susceptibilities are given in units of 10^{-6} erg G^{-2} mol^{-1}, the second moments in $Å^2$, and the molecular electric quadrupole moment, $Q_\parallel$ in DÅ. The latter is referred to the molecular center of mass of the isotopomer.

4. The Anisotropy in the Second Moment of the Electronic Charge Distribution, the Molecular Electric Quadrupole Moment, and the Paramagnetic Susceptibility Perpendicular to the O=C=Se Chain

In Table 2 we also present experimental values for the anisotropy in the second moment of the electronic charge distribution, $\langle \sum b_j^2 - a_j^2 \rangle$, for the molecular electric quadrupole moment referred to the molecular center of mass system, $Q_{aa} = Q_{\|}$, and for the so-called paramagnetic susceptibility perpendicular to the O=C=Se chain, $\xi_{\perp}^{p}$. These quantities were derived in the standard way from the experimental values for $g_{\perp}$, $(\xi_{\|} - \xi_{\perp})$, $B_{\perp}$, $\sum Z_n a_n^2$ under the assumption that their theoretical rigid rotor expressions can be used to a sufficient degree of approximation. For the readers convenience we list the relevant equations. A derivation from first principles has been given in [14], Chapter IV.

$$g_{\perp} = \frac{m_p h}{8\pi^2 B_{\perp}} \left(\sum_{n=1}^{\text{nuclei}} Z_n a_n^2 + \frac{2}{m} \left(\frac{L_b L_b}{\Delta} \right) \right), \tag{2}$$

$$(\xi_{\|} - \xi_{\perp}) = -\frac{N_A e^2}{4mc^2} \left(\left\langle \sum_{j=1}^{\text{electrons}} b_j^2 - a_j^2 \right\rangle + \frac{2}{m} \left(\frac{L_b L_b}{\Delta} \right) \right), \tag{3}$$

$$Q_{aa} = Q_{\|} = |e| \left(\sum_{n=1}^{\text{nuclei}} Z_n a_n^2 + \left\langle \sum_{j=1}^{\text{electrons}} b_j^2 - a_j^2 \right\rangle \right) = \frac{|e| h}{8\pi^2 m_p} \frac{g_{\perp}}{B_{\perp}} - \frac{4mc^2}{|e|} \cdot \frac{1}{N_A} \cdot (\xi_{\|} = \xi_{\perp}), \tag{4}$$

$$\left\langle \sum_{j=1}^{\text{electrons}} (b_j^2 - a_j^2) \right\rangle = \frac{h}{8\pi^2 m_p} \frac{g_{\perp}}{B_{\perp}} - \frac{4mc^2}{N_A e^2} (\xi_{\|} - \xi_{\perp}) - \sum_{n=1}^{\text{nuclei}} Z_n a_n^2 , \tag{5}$$

and

$$\xi_{\perp}^{(p)} = -\frac{e^2 N_A}{2m^2 c^2} \left(\frac{L_b L_b}{\Delta} \right) = -\frac{e^2 N_A}{4mc^2} \left(\frac{h}{8\pi^2 m_p} \frac{g_{\perp}}{B_{\perp}} - \sum_{n=1}^{\text{nuclei}} Z_n a_n^2 \right). \tag{6}$$

Following the arguments presented on p. 104 of [14], we believe that these derived molecular parameters should come close to their vibronic expectation values. In the above equations the brackets, $\langle \ldots \rangle$, indicate electronic matrix elements and $\left(\frac{L_b L_b}{\Delta} \right)$ has been used as a shorthand for the electronic perturbation sum:

$$\left(\frac{L_b L_b}{\Delta} \right) = \sum_{v \neq 0}^{\text{ex. el. states}} \frac{\langle 0 | \hat{L}_b | v \rangle \langle v | \hat{L}_b | 0 \rangle}{E_0 - E_v} \tag{7}$$

with $\hat{L}_b$, the electronic angular momentum operator in direction of the b-axis:

$$\hat{L}_b = \frac{\hbar}{i} \sum_{j=1}^{\text{electrons}} \left(c_j \frac{\partial}{\partial a_j} - a_j \frac{\partial}{\partial c_j} \right). \tag{8}$$

For comparison we have also tried ab initio calculations within the possibilities opened by the Gaussian program package [19]. These calculations were carried out at the spectroscopic equilibrium configuration [17]. As far as the molecular electric quadrupole moment is concerned, the best agreement between the computed and experimental values was obtained in a CID/LANLIDZ+pol calculation. Here CID stands for doubly excited configuration interaction. In this calculation an effective core potential basis set is used at Se [20], supplemented by two sets of polarization functions at each atom with exponents choosen as $\eta_D^{(O,C)} = 1.6$, 0.4 and $\eta_D^{(Se)} = 1.3$, 0.33, respectively. The computed results with respect to the molecular center of mass and with the a-axis pointing from the oxygen atom toward the selenium atom were:

$$Q_{aa,\,\text{calc}} = -0.4001 \text{ DÅ},$$

$$\left\langle \sum^{\text{electrons}} b_j^2 \right\rangle_{\text{calc}} = 5.3042 \text{ Å}^2,$$

$$\left\langle \sum^{\text{electrons}} (b_j^2 - a_j^2) \right\rangle_{\text{calc}} = -60.5733 \text{ Å}^2, \text{ and}$$

$$\mu_{a,\,\text{calc}} = 0.6124 \text{ D}.$$

5. The Orientation of the Electric Dipole Moment

From the change of the $g_{\perp}$ value upon isotopic substitution: $^{80}\text{Se} \rightarrow {}^{78}\text{Se}$ and $^{80}\text{Se} \rightarrow {}^{77}\text{Se}$, we have also computed the molecular electric dipole moment as [21]:

$$\mu_a = -\frac{\hbar |e|}{8\pi m_p \Delta a} \left(\frac{g_{\perp}(^{80}\text{Se})}{B_{\perp}(^{80}\text{Se})} - \frac{g_{\perp}(^{xx}\text{Se})}{B_{\perp}(^{xx}\text{Se})} \right) \tag{9}$$

(with $xx = 77$ or 78). The center of mass shifts with respect to the parent compound $^{16}\text{O}=^{12}\text{C}=^{80}\text{Se}$ lead to $a_n(^{xx}\text{Se}) = a_n(^{80}\text{Se}) + \Delta a$ with $\Delta a = 0.0116$ Å for ^{78}Se substitution and $\Delta a = 0.0175$ Å for ^{77}Se substitution. Together with the tabulated values for $g_{\perp}$ and $B_{\perp}$

this leads to

$$\mu_a(^{80}\text{Se} \rightarrow {}^{78}\text{Se}) = +0.87(41)\ \text{D},$$

$$\mu_a(^{80}\text{Se} \rightarrow {}^{77}\text{Se}) = +0.89(36)\ \text{D}.$$

In both cases the center of mass is shifted towards oxygen, i.e. towards the most electronegative atom. It is therefore not surprising that $g_\perp$ goes positive upon these substitutions. Admittedly the absolute value for μ_a is much less accurate than the value determined earlier in a Stark effect study, $|\mu_a| = 0.752(7)$ D [22], but this merely reflects the fact that in a Zeeman study μ is determined as a difference. However, the improved precision of our MWFT experiment now unambigously confirms the direction of the dipole moment: $\boldsymbol{\mu}$ points from oxygen (negative end) to Se (positive end).

6. Analysis of the Zeeman Splittings in the *l*-Type Doublet States of the Degenerate Bending Vibration

For the analysis of the Zeeman splittings in the first excited states of the degenerate bending vibration ($\tilde{\nu}_2 = 463.6\ \text{cm}^{-1}$, [23]), also known as the *l*-type doublet states, we have used a different theoretical approach. Here we have treated the molecule as slightly bent, i.e. as a near prolate asymmetric top (compare the Appendix) and accordingly we have used the following effective expression for the field dependent energy (cf. [14], Eq. III.13):

$$\langle JK_aK_cM|\,\hat{H}_{\text{Zeeman, eff}}\,|JK_aK_cM\rangle \qquad (10)$$

$$= -\mu_N H_Z \frac{M}{J(J+1)} \sum_\gamma g_{\gamma\gamma} \langle|\hat{J}_\gamma^2|\rangle - \frac{1}{2N_A}\,\xi_{\text{bulk}} H_Z^2$$

$$-\frac{H_Z^2}{N_A} \frac{3M^2 - J(J+1)}{(2J-1)(2J+3)J(J+1)} \sum_\gamma (\xi_{\gamma\gamma} - \xi_{\text{bulk}}) \langle|\hat{J}_\gamma^2|\rangle.$$

The summation index, γ, runs over the three molecular axes *a*, *b*, and *c*, and the brackets, $\langle|\hat{J}_\gamma^2|\rangle$ indicate asymmetric top expectation values for the squares of the angular momentum operators.

Again we assume that the *g*- and ξ-values represent vibrational expectation values of the corresponding rigid rotor expressions.

Within this asymmetric top approach one vibrational degree of freedom is converted into a rotational degree of freedom and the three remaining vibrations, especially the bending vibration, are treated as if occurring in an effective potential, which also accounts for the centrifugal forces arising from the rapid rotation associated with one quantum of rotational angular momentum along the *a*-axis. The stimulation for this treatment comes from the observation that the lowest eigenfunctions of the asymmetric top are symmetrized linear combinations of symmetric top wavefunctions, $|J, K_a, M\rangle$, (⇒ Wang-transformation [24]) and do not depend on the rotational constants. Thus, if one thinks of the rovibrational wavefunctions as products of such an asymmetric top wavefunction and a vibrational function, one quite naturally arrives at *effective* Schrödinger equations for the bending motion. These Schrödinger equations differ slightly for the different low-*J* rotational states. If necessary, especially if vibrational expectation values are of interest, their solutions can be obtained by numerical integration (⇒ Numerov-Cooley method [25, 26]). For more details see the Appendix.

Our observed Zeeman multiplet frequencies are given in Table 3. Unfortunately and for yet unknown reasons the upper doublet could not be analysed with the same high resolution as the lower doublet, and thus not all five Zeeman-parameters (three *g*-values and two susceptibility anisotropies) could be determined independently. We therefore deliberately set $g_{bb} = g_{cc} = g_\perp$ and we also used $\xi_{bb} = \xi_{cc} = \xi_\perp$. In other words, we only fitted two *g*-values, $g_\perp$ and $g_\parallel$, and one susceptibility anisotropy, $(\xi_\parallel - \xi_\perp)$, to the observed Zeeman splittings. Most likely these approximations come very close to reality. First, the observed Zeeman pattern of the upper doublet transition nicely agrees with the prediction from the values for $g_\perp$, $g_\parallel$, and $(\xi_\parallel - \xi_\perp)$ all three fitted to the well resolved Zeeman multiplet of the lower doublet transition, and second, in a study of the related molecule OCS [27], the perpendicular *g*-values, g_{bb} and g_{cc}, and the corresponding susceptibilities ξ_{bb} and ξ_{cc} were indeed found to agree within better than 1% of their values. In Table 4 we present our two *g*-values and the susceptibility anisotropy for the $v_2 = 1, l = \pm 1$ state (in conventional notation) or (in our notation) for the low-*J* rotational states with $K_a = 1$: 1_{11}, 1_{10}, 2_{12}, and 2_{11} of the effectively bent molecule.

We note that the $g_\perp$ and $(\xi_\parallel - \xi_\perp)$ values in the effectively bent $v_2 = 1$ state are not very different form their counterparts in the linear configuration of the vibrational ground state. What is new is the nonzero $g_{aa} = g_\parallel$ value. It includes a nuclear and an electronic

Table 3. Zeeman multiplets of the $J' = 2 \rightarrow J'' = 1$ rotational transitions of $^{16}O^{12}C^{80}Se$ in the so-called l-type doublet of the first excited state of the bending vibration, both observed in a magnetic field of 20010(5) Gauss = 2.0010(5) Tesla. M'' and M' denote the M-values of the lower and upper state, respectively. ν_0 denotes the zero field frequencies. All frequencies are given in kHZ.

Isotopomer M''	(v_1, v_2, v_3) M'	$\nu_{0,\mathrm{exp}}$ $\nu_{H,\mathrm{exp}}$	$J'_{K'_a K'_c}$ $\Delta\nu_{\mathrm{exp}}$	$\rightarrow$ $\Delta\nu_{\mathrm{calc}}$	$J''_{K''_a K''_c}$ $\delta\nu$	Rel. *Int.* %
$OC^{80}Se$	$(0, 1^{(-1)}, 0)$	16 091 876.8	2_{12}	$\rightarrow$	1_{11}	
−1	−2	16 091 423.4	−453.3	−453.1	−0.2	100.0
0	−1	16 091 729.5	−147.2	−147.5	0.3	50.0
1	0	16 091 783.7	−93.0	−94.1	+1.1	16.5
−1	0	16 091 998.3	+121.6	+123.1	−1.5	16.5
+1	+2	16 092 165.0	+288.3	+288.2	+0.1	100.0
0	+1	16 092 209.6	+332.9	+331.8	+1.1	50.0
$OC^{80}Se$	$(0, 1^{(+1)}, 0)$	16 104 565.4	2_{11}	$\rightarrow$	1_{10}	
−1	−2	16 104 110.8	−454.6	−453.1	−1.5	100.0
0	−1	16 104 417.8	−147.6	−147.5	−0.1	50.0
+1	0	–	–	−94.1	–	16.5
−1	0	–	–	+123.1	–	16.5
+1	+2	16 104 851.9	+286.5	+288.2	−1.7	100.0
0	+1	16 104 898.1	+332.7	+331.8	+0.9	50.0

Table 4. Molecular g-values and susceptibility anisotropy of $^{16}O^{12}C^{80}Se$ in the l-type doublet state with $v_2 = 1$, $l = -1$. The susceptibility anisotropy is given in units of 10^{-6} erg G^{-2} mol^{-1}.

$g_\perp$	$g_\parallel$	$\xi_\parallel - \xi_\perp$
−0.02002(3)	+0.00575(15)	−10.152(82)

contribution as given by (11) (cf. (I,2) in [14]):

$$g_{aa} = \langle \Phi_v(\beta) | \frac{m_p \sum Z_n b_n^2}{\sum m_n b_n^2} | \Psi_v(\beta) \rangle + m_p \langle \Psi_v(\beta) | \frac{2\left(\frac{L_a L_a}{\Delta}\right)}{m \sum m_n b_n^2} | \Psi_v(\beta) \rangle . \quad (11)$$

In (11) the brackets, $\langle \Psi_v(\beta) | \ldots | \Psi_v(\beta) \rangle$, denote ground state expectation values with respect to the bending vibration.

If one approximates the functional dependence on the bending angle, β, in both expectation values by the leading term in the corresponding Taylor expansion, i.e. by:

$$b_n(\beta) \simeq b'_n(0) \cdot \beta \quad (12)$$

and

$$\left(\frac{L_a L_a}{\Delta}\right)_{(\beta)} \simeq \frac{1}{2!} \left(\frac{L_a L_a}{\Delta}\right)''_{(0)} \cdot \beta^2 , \quad (13)$$

where the primes indicate derivatives with respect to β, (11) leads to the following estimates for $g_{aa,\,\mathrm{nucl}}$ and for the second derivative of the perturbation sum, respectively:

$$g_{aa,\,\mathrm{nucl}} = \frac{m_p \sum Z_n b'^2_n(0)}{\sum m_n b'^2_n(0)} = 0.5022_{51} , \quad (14)$$

$$\frac{\partial^2}{\partial \beta^2} \left(\frac{L_a L_a}{\Delta}\right) \simeq (g_{aa\,\mathrm{exp}} - g_{aa\,\mathrm{nucl}}) \frac{m \sum m_n b'^2_n(0)}{m_p} = -1.1956 \cdot 10^{-3} \frac{\mathrm{amu\ \AA^2}}{\mathrm{rad^2}} . \quad (15)$$

In (14) and (15) we have used the rigid bender approximation for the calculation of $\sum m_n b'^2_n(0) = 4.4214$ amu $Å^2/rad^2$ and $\sum Z_n b'^2_n(0) = 2.2046$ $Å^2/rad^2$, respectively. For details see the Appendix.

Within the above parabolic approximation for the second order electronic perturbation sum we can predict the paramagnetic susceptibility, $\xi^{(p)}_{aa}$, for not too large bending angles as:

$$\xi^{(p)}_{aa} = -N_A \cdot \frac{e^2}{2m^2 c^2} \cdot \frac{1}{2!} \left(\frac{L_a L_a}{\Delta}\right)'' \cdot \beta^2 = 9.246 \cdot 10^{-6} \cdot \beta^2 \frac{\mathrm{erg}}{\mathrm{G^2\ mol\ rad^2}} .$$

Using the analytical solution for the Schrödinger equation of the bending vibration (see the Appendix), we can also give the vibrational ground state expectation value for β^2 in the $K_a = 1$ states as:

$$\langle \beta^2 \rangle = \frac{\hbar}{\pi c \bar{\nu}_2^0 \sum m_n b'_n(\beta=0)^2} = 0.0329\ \mathrm{rad^2} .$$

We finally note that with a value of −0.4965 the electric contribution to g_{aa} comes very close to the corre-

sponding value reported for the related molecule OCS [27] where $g_{aa,\,\mathrm{elec\,(OCS)}} = -0.4404(5)$ has been found.

7. The Missing Translation Stark Effect in the Transient Emission Signals from the *l*-Type Doublets

We now turn to an interesting feature of the microwave Fourier transform technique used in the present investigation. It originates from the translational or Lorentz-Stark-effect. This effect leads to velocity dependent shifts of the Zeeman levels and was neglected in our analysis of the Zeeman splittings. We first recall the physics behind the translational Stark effect and present a simulation of the *l*-type doublet Zeeman patterns such as they should be observable by frequency domain microwave spectroscopy. Then we indicate, why it appears reasonable that the Zeeman multiplet frequencies of our time domain spectroscopic study do not show any peculiarities which might be attributed to the translational Stark effect.

We start with the general discussion. The notion "translational Stark effect" has been coined to relate the perturbations caused by the Lorentz forces associated with the center of mass motion to the more familiar perturbations by an exterior electric field. For molecules which have a nonzero component of the center of mass velocity perpendicular to the magnetic field $\boldsymbol{v}_\perp$, the corresponding contribution to the Lorentz forces, which act on the molecular electric charge distribution, are given by:

$$\boldsymbol{F}_i = \frac{1}{c} q_i (\boldsymbol{v}_\perp \times \boldsymbol{H}_Z) \,. \tag{16}$$

Here q_i represents the i-th point charge within the molecule, i.e. $-e$ if it is an electron, or $+Z_i e$, if it is a nucleus. Obviously these Lorentz forces can be minimiced by a fictitious electric field of size:

$$\boldsymbol{E}_{\mathrm{Lorentz}} = \frac{1}{c} (\boldsymbol{v}_\perp \times \boldsymbol{H}_Z) \tag{17}$$

and they lead to a Stark-effect type additional energy contribution which may also be written as:

$$\hat{H}_{\mathrm{Lorentz\text{-}Stark}} = -\boldsymbol{\mu} \cdot \boldsymbol{E}_{\mathrm{Lorentz}} \,. \tag{18}$$

In (18) $\boldsymbol{\mu}$ is the vibronic ground state expectation value of the molecular electric dipole moment. Since the corresponding electric fields are small, only a few V/cm at typical thermal velocities, they can usually be neglected. They only have to be accounted for in systems which exhibit fast Stark effects, i.e. systems in which already small electric fields lead to detectable Stark shifts of the energy levels. Examples for such systems are symmetric tops, molecules with nearly free methyl top internal rotation, and also linear molecules in the *l*-doublet states of degenerate bending vibrations, such as in OCSe studied here. In the latter case, the fast Stark effect is caused by the narrow energy spacings within the doublets and by the fact that a Stark-effect matrix element associated with the nonzero a-component of the molecular electric dipole moment connects the near degenerate levels.

In the following we will use our asymmetric top notation for the effectively bent molecule, i.e. we will address the doublets as K_a-doublets rather than *l*-type doublets. In the case of $^{16}O^{12}C^{80}Se$ the doublet spacings (in frequency units) are only 6.344 MHz in the $J=1$ doublet i.e. between the $1_{1,1}$ and the $1_{1,0}$ asymmetric top levels, and only $3 \cdot 6.344$ MHz in the $J=2$ doublet, i.e. between the $2_{1,2}$ and the $2_{1,1}$ levels. The corresponding asymmetric top Stark effect matrix elements are easily calculated from the known symmetric top matric elements for the direction cosine between the molecular a-axis and the direction of $\boldsymbol{E}_{\mathrm{Lorentz}}$ (cf. [24], Table 2.1). They are given by (19):

$$\langle JK_aK_cM \,|\, \cos(a, X) \,|\, JK_aK_c - 1\, M \pm 1 \rangle = \frac{K_a \sqrt{J(J+1) - M(M \pm 1)}}{2J(J+1)} \tag{19}$$

with $K_a = 1$ and $J = 1$ or 2, depending on whether the $J=1$ or the $J=2$ K_a-doublet is considered. Here, in order to avoid complex numbers, we have used an individual choice of laboratory axes for each absorber molecule. All these coordinate systems have a common direction for the Z-axis. It points into the direction of the magnetic field. But the X-axes are chosen individually to point in the direction of $\boldsymbol{E}_{\mathrm{Lorentz}}$ as determined by $\boldsymbol{v}_\perp$ of the molecule under consideration.

To estimate the energy shifts caused by the translational Stark effect one can use second order perturbation theory. This approach is fine for moderate thermal velocities, which correspond to Stark effect matrix elements on the order to 1 MHz or below in frequency units. It is insufficient for molecules with high velocities perpendicular to the magnetic field, but those are few anyhow. Obviously the translational Stark effect perturbation pushes the M-levels of the lower level in

the doublet to lower energies and those of the higher level to higher energies and this second order shift is larger in the more narrowly spaced $J=1$ doublet than in the wider spaced $J=2$ doublet. Since the electric dipole transitions of interest here are $1_{1,1} \leftrightarrow 2_{1,2}$ and $1_{1,0} \leftrightarrow 2_{1,1}$ i.e. lower $\leftrightarrow$ lower and upper $\leftrightarrow$ upper, the translational Stark effect will shift the Zeeman satellites of the high frequency multiplet (upper to upper) to lower frequencies and those of the low frequency multiplet (lower to lower) to higher frequencies. Furthermore the magnitude of these shifts will be proportional to the square of $v_\perp$ as long as the second order perturbation theory is sufficient. In Fig. 2 we present simulated Zeeman multiplets for OCSe. For the simulation the continuous two dimensional velocity distribution of the absorber molecules was discretizised, i.e. all absorber molecules within a $v_\perp$-interval of 10 m/sec were grouped together as if travelling at the center velocity of the interval. Then the $J=1$ blocks and the $J=2$ blocks which correspond to the K_a-doublets of the effective asymmetric top Hamiltonian including the translational Stark effect matrix elements were diagonalized numerically and the direction cosine matrix was subjected to the corresponding unitary transformation for the correct dipole transition intensities. Finally the intensities were weighted according to the two dimensional Boltzmann distribution assuming a temperature of -65 °C. This procedure is basically the same as was used earlier by Hüttner, Bodenseh, and Nowicki [3] in their analysis of the rotational Zeeman effect in the *l*-type doublets of HCCF, and also the simulations look very similar. From Fig. 2 one would expect that the observed satellite frequencies should be corrected for the frequency shifts due to the translational Stark effect prior to an analysis according to the energy expression presented in (10).

Initially we tried such a correction. But it leads to a large discrepancy in the values for the susceptibility anisotropy if the latter is determined from the shift of the center frequency of the $M=1 \leftrightarrow 2$, $M=-1 \leftrightarrow -2$ Zeeman doublet with respect to the zero field frequency on the one hand or from the corresponding shift of the $M=0 \leftrightarrow 1$, $0 \leftrightarrow -1$ Zeeman doublet on the other hand. (The latter are expected to be perturbed twice as much as the former, compare too Figure 2). Also the broadening of the lines, albeit asymmetric, which is caused by the translational Stark effect, should translate into seemingly shorter relaxation times in the time domain signals. Nothing like that was observed. Obviously the effect of the translational

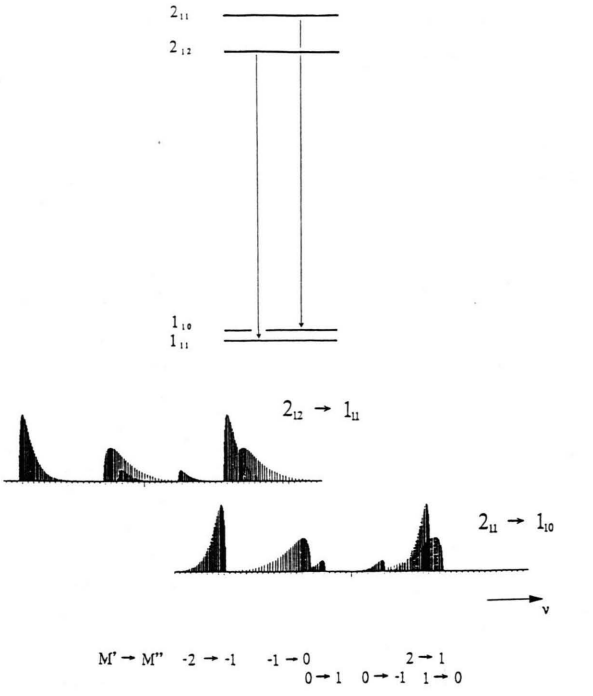

Fig. 2. Simulation of the perturbations of the Zeeman multiplets in the *l*-type doublets by the "translational Stark-effect" (see text). At left we present a schematic drawing of the energy level scheme. The shading of the absorption lines is caused by the fast second order Stark-effect type perturbation which is associated with the direction cosine matrix elements connecting the closely spaced doublets. The energy levels are designated by the corresponding asymmetric top quantum numbers. In our MWFT-experiment no shading could be observed, since sampling of the transient emission signal started with a delay of about 2 μs. During this time interval between the end of the pulse and the start of data sampling most fast moving molecules, i.e. those that are heavily perturbed by the translational Stark-effect, have already suffered a coherence destroying collision and do no more contribute to the detected signal.

Stark effect on the observed transient emission signals was minute.

Our interpretation of this finding is as follows. Because of electronic perturbations associated with the generation of the intense microwave pulse we did not start data collection immediately after the end of the pulse but after a delay of approximately 1.8 μsec. In the mean time most of those absorber molecules, which travel with high velocity components perpendicular to the magnetic field and thus emit resonance frequencies heavily perturbed by the translational Stark effect, have already undergone a coherence destroying collision and thus can no more contribute to the transient emission signal. Not only gas–gas colli-

sions but also wall collisions have to be accounted for in this context. With only about 0.24 cm to go from the center of the Ku-band waveguide to the wall, it takes only about 8 μsec until a molecule which travels at a speed of 300 m/sec perpendicular to the wall collides with the latter. Thus such a molecule can contribute to the transient emission signal only during the first quarter of the sampling period. Only molecules travelling along the axis of the waveguide are not subjected to sudden memory loss due to a wall collision. But their emission signals rapidly decay due to Doppler dephasing. We therefore conclude that the transient emission signal observed after a delay of about 2 μsec largely arises from molecules with low translational velocities $v_\perp$. Together with the fact that the "Lorentz frequency shifts" go proportional to $v_\perp^2$ this easily explaines why frequency shifts due to the translational Stark effect could not be observed in our experiments. On the other hand, since the translational Stark effect directly probes the translational velocity of the molecules, it might be interesting to use it to gain extra information in studies of the velocity dependence of collisional cross sections and relaxation rates.

The physical picture developed here also suggests that in frequency domain Zeeman spectra of *l*-type doublets the translational Stark effect shading of the Zeeman satellites should be more pronounced in the $\Delta M = 0$ configuration than in the $\Delta M = \pm 1$ configuration, at least as long as the pressure is so low that wall collision broadening dominates. The idea behind this expectation is that in the $\Delta M = 0$ configuration $v_\perp$ is directed parallel to the broad face of the waveguide. Thus the absorption lines of high speed molecules with a correspondingly large perturbation due to the translational Stark effect will suffer less wall collision broadening. As a result their superpositions will trace the asymmetrically shaded line profile deduced from the two dimensional Boltzmann distribution more faithfully.

8. Appendix: The Rotational Zeeman Effect of the Triatomic Bender

8.1. The Classical Lagrangian of the Rigid Bender in an Exterior Magnetic Field

In the following we outline a simplified treatment of the rotational Zeeman effect of triatomic molecules. We use the model of the semirigid bender. Within this model the molecule is represented by three (atomic) point masses, in our case with masses m_O, m_C, and m_{Se}, each with an effective electric charge, q_O, q_C, q_{Se}, attached to it. The presence of the electrons is accounted for only in so far as they are assumed to contribute to the point charges (one might think of Mulliken charges). They are also assumed to provide the intramolecular potential energy, $V_{(r_{(O=C)}, r_{(C=Se)}, \beta)}$, as a function of the bond distances and the bond angle, β. The explicit inclusion of the electrons, which also allows for a theoretical description of the susceptibilities, is briefly sketched at the end of this Appendix. The starting point of our theoretical treatment is the Lagrangian for this three body model in an exterior magnetic field, $\boldsymbol{H}$. If referred to the laboratory frame, this Lagrangian may be written as [28]:

$$L = \frac{1}{2} \sum_{n=O,C,Se} m_n \boldsymbol{V}_n^2 + \frac{1}{c} \sum_{n=O,C,Se} q_n \boldsymbol{V}_n \cdot \boldsymbol{A}_n - V_{(r_{(O=C)}, r_{(C=Se)}, \beta)} . \quad (20)$$

In (20) $\boldsymbol{V}_n$ is the velocity of the n-th particle with respect to the laboratory frame. $\boldsymbol{A}_n$ is the vector potential of the exterior field at the position of the n-th particle. c is the velocity of light (to facilitate the comparison with the literature we use the cgs-system throughout).

For simplification we will treat the center of mass motion classically, i.e. we assume that the position of the molecular center of mass is described by:

$$\boldsymbol{R}_{c.m.} = \boldsymbol{R}_c + \boldsymbol{V}_{c.m.} t . \quad (21)$$

In (21) $\boldsymbol{R}_c$ denotes the position at the moment of the last collision and $\boldsymbol{V}_{c.m.}$ denotes the center of mass velocity of the molecule with respect to the Laboratory frame. We will use capital letters for vectors referred to the laboratory system.

We now introduce an intermolecular cartesian center of mass coordinate system with unit basis vectors $\boldsymbol{e}_a$, $\boldsymbol{e}_b$, $\boldsymbol{e}_c$ (see Figure A.1). As internal molecular coordinate system we use a system which, for small bending angles, comes close to the instantaneous principal inertia axes system. (Later we will specify the $\boldsymbol{e}_a$, $\boldsymbol{e}_b$, $\boldsymbol{e}_c$ system by imposing the condition that the intramolecular angular momentum associated with the bending vibration vanishes [29].)

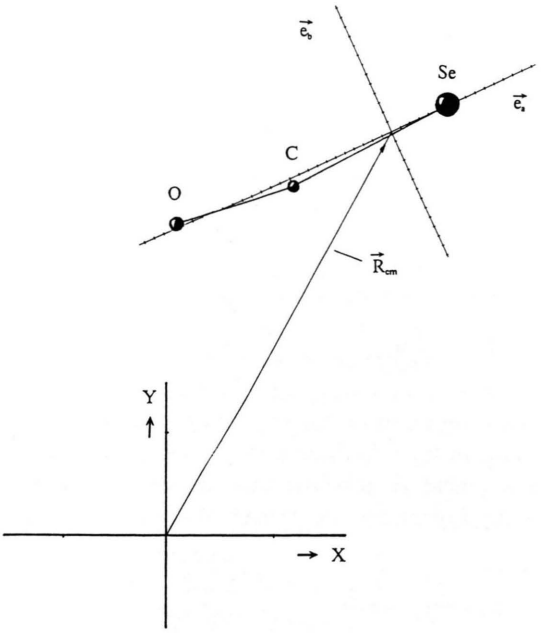

Fig. A.1. Coordinate systems used in the derivation of the Hamiltonian for the rigid bender. The molecular coordinate system is defined such that there is no intramolecular angular momentum associated with the bending motion. At small bending angles it almost coincides with the instantaneous principal axes system (compare [29]).

We now rewrite the Lagrangian with reference to the molecular center of mass system. With

$$\boldsymbol{R}_n = \boldsymbol{R}_{\text{c.m.}} + \boldsymbol{r}_n\,, \quad \boldsymbol{V}_n = \boldsymbol{V}_{\text{c.m.}} + \boldsymbol{v}_n\,, \tag{22}$$

the Lagrangian takes the form:

$$\begin{aligned} L = {} & \tfrac{1}{2}\sum_n m_n V_{\text{c.m.}}^2 + \tfrac{1}{2}\sum_n m_n v_n^2 \\ & + \frac{1}{2c}\sum_n q_n V_{\text{c.m.}} \cdot (\boldsymbol{H} \times \boldsymbol{R}_{\text{c.m.}}) \\ & + \frac{1}{2c}\sum_n q_n V_{\text{c.m.}} \cdot (\boldsymbol{H} \times \boldsymbol{r}_n) \\ & + \frac{1}{2c}\sum_n q_n \boldsymbol{v}_n \cdot (\boldsymbol{H} \times \boldsymbol{R}_{\text{c.m.}}) \\ & + \frac{1}{2c}\sum_n q_n \boldsymbol{v}_n \cdot (\boldsymbol{H} \times \boldsymbol{r}_n) - V_{(r_{(O=C)}, r_{(C=Se)}, \beta)}\,. \end{aligned} \tag{23}$$

In the following we drop the first term in (23), i.e. the kinetic energy associated with the translation of the molecule as a whole. Within our model it is constant between collisions and thus has no spectroscopic relevance. Furthermore we note that the third sum in (23) vanishes due to the electroneutrality condition: $\sum_n q_n = 0$. Third we note that the fifth sum in (23) suggests an explicit dependence on the molecular position in space which is clearly unphysical as long as the molecule is in the homogeneous region of the magnetic field and which indeed can be removed. To this end we exploit the equivalence of all Lagrangians which only differ by the total derivative with respect to time of a function of the coordinates and time [30]:

$$\tilde{L} \simeq L - \frac{\mathrm{d}\Phi(\ldots, \boldsymbol{R}_n \ldots, t)}{\mathrm{d}t}\,. \tag{24}$$

For comparison of the fifth sum in (23) we choose Φ as:

$$\Phi = +\frac{1}{2c}\sum_n q_n (\boldsymbol{H} \times \boldsymbol{R}_{\text{c.m.}}(t)) \cdot (\boldsymbol{R}_{\text{c.m.}}(t) + \boldsymbol{r}_n)\,. \tag{25}$$

With the explicit time dependence of $\boldsymbol{R}_{\text{c.m.}}$ as given in (21) this leads to:

$$\begin{aligned} \frac{\mathrm{d}\Phi}{\mathrm{d}t} = {} & \frac{1}{2c}\sum_n q_n (\boldsymbol{H} \times \boldsymbol{V}_{\text{c.m.}}) \cdot (\boldsymbol{R}_{\text{c.m.}}(t) + \boldsymbol{r}_n) \\ & + \frac{1}{2c}\sum_n q_n (\boldsymbol{H} \times \boldsymbol{R}_{\text{c.m.}}(t)) \cdot \boldsymbol{V}_{\text{c.m.}} \\ & + \frac{1}{2c}\sum_n q_n (\boldsymbol{H} \times \boldsymbol{R}_{\text{c.m.}}(t)) \cdot \boldsymbol{v}_n\,. \end{aligned} \tag{26}$$

In (26) the last sum is used to compensate the explicit $\boldsymbol{R}_{\text{c.m.}}$-dependence in (23). The second sum vanishes due to the electroneutrality condition. The same is true for part of the first sum. The second part in the first sum adds to the fourth contribution in the original Lagrangian (23) and we end up with:

$$\begin{aligned} \tilde{L} = {} & \tfrac{1}{2}\sum_n m_n v_n^2 + \frac{1}{c}\sum_n q_n \boldsymbol{r}_n \cdot (\boldsymbol{V}_{\text{c.m.}} \times \boldsymbol{H}) \\ & + \frac{1}{2c}\sum_n q_n \boldsymbol{v}_n \cdot (\boldsymbol{H} \times \boldsymbol{r}_n) - V_{(r_{(O=C)}, r_{(C=Se)}, \beta)}\,. \end{aligned} \tag{27}$$

In (27) the second sum can be minimized by the Coulomb energy of the "molecular charge distribution" in a fictitious exterior electric field of size

$$\boldsymbol{E}_{\text{Lorentz}} = \frac{1}{c}(\boldsymbol{V}_{\text{c.m.}} \times \boldsymbol{H})\,. \tag{28}$$

For later use we will address this Coulomb energy as $V_{\text{Coulomb-Lorentz}}$:

$$V_{\text{Coulomb-Lorentz}} = -\sum_n q_n \boldsymbol{r}_n \cdot \frac{1}{c}(\boldsymbol{V}_{\text{c.m.}} \times \boldsymbol{H}) = -\boldsymbol{\mu}_{\text{electr}} \cdot \boldsymbol{E}_{\text{Lorentz}} \cdot \tag{29}$$

As the next step we break down the velocity vectors of the three point masses with respect to the center of mass, $\boldsymbol{v}_n$, into an intramolecular (vibrational) contribution and a contribution due to the overall rotation of the three body system. To this end we write the position vectors $\boldsymbol{r}_n$ explicitly as:

$$\boldsymbol{r}_n = a_n \boldsymbol{e}_a + b_n \boldsymbol{e}_b + c_n \boldsymbol{e}_c \,. \tag{30}$$

We obtain

$$\boldsymbol{v}_n = \frac{\mathrm{d}\boldsymbol{r}_n}{\mathrm{d}t} = \dot{a}_n \boldsymbol{e}_a + \dot{b}_n \boldsymbol{e}_b + \dot{c}_n \boldsymbol{e}_c + a_n \dot{\boldsymbol{e}}_a + b_n \dot{\boldsymbol{e}}_b + c_n \dot{\boldsymbol{e}}_c \,. \tag{31}$$

The dots indicate derivatives with respect to time. Since the time derivatives of the basis vectors of a gyrating coordinate system may be written as vector products with the corresponding instantaneous angular velocity $\boldsymbol{\omega}$,

$$\dot{\boldsymbol{e}}_g = (\boldsymbol{\omega} \times \boldsymbol{e}_g) \quad (g = a, b, c)\,, \tag{32}$$

we can rewrite $\boldsymbol{v}_n$ as:

$$\boldsymbol{v}_n = \boldsymbol{v}_{n\,\text{rel}} + (\boldsymbol{\omega} \times \boldsymbol{r}_n) = \boldsymbol{v}_{n\,\text{vib}} + \boldsymbol{v}_{n\,\text{rot}} \,, \tag{33}$$

where

$$\boldsymbol{v}_{n\,\text{rel}} = \dot{a}_n \boldsymbol{e}_a + \dot{b}_n \boldsymbol{e}_b + \dot{c}_n \boldsymbol{e}_c = \boldsymbol{v}_{n\,\text{vib}} \,.$$

With explicit reference to the vibrational and rotational origin of its contributions the Lagrangian finally becomes:

$$\begin{aligned} \tilde{L} = {} & \tfrac{1}{2}\sum_n m_n \boldsymbol{v}_{n\,\text{rel}}^2 + \sum_n m_n \boldsymbol{v}_{n\,\text{rel}}(\boldsymbol{\omega} \times \boldsymbol{r}_n) + \tfrac{1}{2}\sum_n m_n (\boldsymbol{\omega} \times \boldsymbol{r}_n)^2 \\ & + \frac{1}{2c}\sum_n q_n \boldsymbol{v}_{n\,\text{rel}} \cdot (\boldsymbol{H} \times \boldsymbol{r}_n) \\ & + \frac{1}{2c}\sum_n q_n (\boldsymbol{\omega} \times \boldsymbol{r}_n) \cdot (\boldsymbol{H} \times \boldsymbol{r}_n) \\ & - V_{(r_{(O=C)}, r_{(C=Se)}, \beta)} - \boldsymbol{\mu}_{\text{electr}} \cdot \boldsymbol{E}_{\text{Lorentz}} \cdot \end{aligned} \tag{34}$$

As the next step we adopt the rigid bender approximation, i.e. we freeze the bond distances $r_{(O=C)}$ and $r_{(C=Se)}$ at their equilibrium values. This leaves us with only one internal (vibrational) degree of freedom, the bending angle β. Furthermore we specify the molecular center of mass coordinate system such that its a/b-plane equals the plane spanned by the two bonds. We also define the orientation of the a-axis with respect to the C=Se-bond such that there is no intramolecular angular momentum associated with the bending motion (see [29]):

$$\sum_n^{\text{point masses}} m_n (\boldsymbol{r}_n \times \boldsymbol{v}_{n\,\text{rel}}) = 0 \,. \tag{35}$$

This choice of intramolecular coordinate system eliminates the second sum in (34), (i.e. the so-called Coriolis interaction) and thus further simplifies the Lagrangian. In field free space this model has been treated in detail by Hougen, Bunker, and Johns [29] and we refer to their Eq. (4) for the orientation of the intramolecular center of mass system with respect to the instantaneous direction of the C → Se bond.

Next we introduce angular momenta:

$$P_g = \frac{\partial L}{\partial \omega_g} \quad (g = a, b, c)\,, \quad P_\beta = \frac{\partial L}{\partial \dot{\beta}} \,. \tag{36}$$

Strictly the Eulerian angular velocities should have been used rather than the omegas and the corresponding Eulerian angular momenta rather than the P_g defined in (36), but it can be shown that our simplified treatment leads to the correct result [31]. In the following section we will use these angular momenta to construct the classical Hamiltonian for our model. Finally we will translate the classical Hamiltonian into quantum mechanics.

8.2. The Classical Hamiltonian

From the Lagrangian and the definition of the momenta corresponding to the "velocities" $\dot{q}_k$ (in our case: ω_a, ω_b, ω_c, and $\dot{\beta}$), we then obtain the classical Hamiltonian as (cf. Chapter A.V. § 2 in [28]):

$$H = \sum_k P_k \dot{q}_k - L \,, \tag{37}$$

where $\dot{q}_k$ and P_k are used for the four angular velocities and the corresponding angular momenta, respectively. For the explicit formulation of the Hamiltonian it is helpful to introduce a compact matrix notation. (In the following bold print face will be used to denote matrices.) To this end we define one-column matrices for the angular velocities, $\boldsymbol{\Omega}$ and angular momenta, $\mathbf{P}$, respectively, with the corresponding transposed (one

row) matrices defined as follows:

$$\boldsymbol{\Omega}^t = (\omega_a, \omega_b, \omega_c, \dot{\beta}),$$
$$\mathbf{P}^t = (P_a, P_b, P_c, P_\beta). \tag{38}$$

We also introduce a generalized four by four moment of inertia matrix, **I**, and a one-column "Zeeman matrix", **Z**, whose elements depend on the electric charge distribution and, linearly, on the magnetic field strength, H_Z.

The components of **I** and **Z** may be deduced from (34) by matrix multiplications if the vector products are expressed as matrix products such as for instance:

$$(\boldsymbol{\omega} \times \boldsymbol{r}_n) = \begin{pmatrix} 0 & (c_n = 0) & -b_n \\ (-c_n = 0) & 0 & a_n \\ +b_n & -a_n & 0 \end{pmatrix} \cdot \begin{pmatrix} \omega_a \\ \omega_b \\ \omega_c \end{pmatrix}. \tag{39}$$

With this notation the Lagrangian may be written as:

$$\tilde{L} = \tfrac{1}{2}\,\boldsymbol{\Omega}^t \cdot \mathbf{I} \cdot \boldsymbol{\Omega} + \boldsymbol{\Omega}^t \cdot \mathbf{Z} - V_{(\beta)} - V_{\text{Coulomb-Lorentz}}. \tag{40}$$

Insertion of

$$\mathbf{P} = \mathbf{I} \cdot \boldsymbol{\Omega} + \mathbf{Z} \tag{41}$$

and

$$\boldsymbol{\Omega} = \mathbf{I}^{-1} \cdot (\mathbf{P} - \mathbf{Z}) \tag{42}$$

into (37) leads to the Hamiltonian as:

$$H = \tfrac{1}{2}(\mathbf{P} - \mathbf{Z})^t \cdot \mathbf{I}^{-1} \cdot (\mathbf{P} - \mathbf{Z}) + V_{(\beta)} + V_{\text{Coulomb-Lorentz}}. \tag{43}$$

In (42) and (43) $\mathbf{I}^{-1}$ represents the inverse of **I**.

The explicit expressions for **I**, $\mathbf{I}^{-1}$ are as follows:

$$\mathbf{I} = \begin{pmatrix} I_{aa} & I_{ab} & 0 & 0 \\ I_{ab} & I_{bb} & 0 & 0 \\ 0 & 0 & I_{cc} & 0 \\ 0 & 0 & 0 & I_{\beta\beta} \end{pmatrix}, \tag{44}$$

$$\mathbf{I}^{-1} = \begin{pmatrix} I_{bb}/D & -I_{ab}/D & 0 & 0 \\ -I_{ab}/D & I_{bb}/D & 0 & 0 \\ 0 & 0 & 1/I_{cc} & 0 \\ 0 & 0 & 0 & 1/I_{\beta\beta} \end{pmatrix}. \tag{45}$$

The following shorthand notation is used:

$$I_{aa} = \sum_n m_n b_n^2, \quad I_{ab} = -\sum_n m_n a_n b_n, \quad I_{bb} = +\sum_n m_n a_n^2,$$
$$I_{cc} = \sum_n m_n (a_n^2 + b_n^2), \quad I_{\beta\beta} = \sum_n m_n (a_n b_n' - b_n a_n'). \tag{46}$$

The prime indicates a derivative with respect to the bending angle β, i.e. $b_n' = \dfrac{\mathrm{d}b_n(\beta)}{\mathrm{d}\beta}$ etc. The letter D is used for the determinant of the 2×2 submatrix in the upper left corner of **I**:

$$D = (I_{aa} I_{bb} - I_{ab} I_{ab}). \tag{47}$$

The explicit expression for **Z** is given by

$$\mathbf{Z} = \begin{pmatrix} Z_a \\ Z_b \\ Z_c \\ Z_\beta \end{pmatrix} = \tag{48}$$

$$= \begin{pmatrix} \frac{1}{2c}\sum_n q_n b_n^2 \cos(aZ) - \frac{1}{2c}\sum_n q_n a_n b_n \cos(bZ) \\ -\frac{1}{2c}\sum_n q_n a_n b_n \cos(aZ) + \frac{1}{2c}\sum_n q_n a_n^2 \cos(bZ) \\ \frac{1}{2c}\sum_n q_n (a_n^2 + b_n^2) \cos(cZ) \\ \frac{1}{2c}\sum_n q_n (a_n b_n' - b_n a_n') \cos(cZ) \end{pmatrix} \cdot H_Z.$$

We now split the classical Hamiltonian into the zero field Hamiltonian and the Zeeman contribution:

$$\begin{aligned} H = {} & \tfrac{1}{2}\mathbf{P}^t \cdot \mathbf{I}^{-1} \cdot \mathbf{P} + V_{(\beta)} \\ & - \tfrac{1}{2}(\mathbf{Z}^t \cdot \mathbf{I}^{-1} \cdot \mathbf{P} + \mathbf{P}^t \cdot \mathbf{I}^{-1} \cdot \mathbf{Z}) \\ & + \tfrac{1}{2}\mathbf{Z}^t \cdot \mathbf{I}^{-1} \cdot \mathbf{Z} \\ & - \boldsymbol{\mu}_{\text{electr}} \cdot \boldsymbol{E}_{\text{Lorentz}}. \end{aligned} \tag{49}$$

This Hamiltonian has to be translated into quantum mechanics and the corresponding eigenvalue problem has to be solved. In fields of up to 2 Tesla (20 kG) the zero field Hamiltonian (first row in (49)) clearly dominates and the Zeeman contributions (second through fourth row) may be treated by perturbation theory. The second row which is linear in the field strength, H_Z, will lead to a contribution which is conventionally attributed to the molecular g-tensor. The third row is proportional to H_Z^2 and corresponds to a susceptibility contribution.

8.3. Translation of the Classical Hamiltonian into Quantum Mechanics

We first treat the zero field Hamiltonian. Explicitly written the classical zero field Hamiltonian has the following form:

$$H_0 = \frac{1}{2}\frac{1}{I_{\beta\beta}} P_\beta^2 + V_{(\beta)} + \frac{I_{bb}}{2D} P_a^2 + \frac{I_{aa}}{2D} + \frac{1}{2I_{cc}} P_c^2 - \frac{I_{ab}}{2D}(P_a P_b + P_b P_a) \tag{50}$$

with D defined in (47).

For simplification and to work out the general line of thought more clearly, we approximate this expression by setting the off diagonal element I_{ab} to zero. Actually this is a fairly good approximation since I_{ab} starts out with zero for $\beta=0$ and stays close to zero up to rather large bending angles as is demonstrated in Figure A.2. The figure suggests that $I_{ab}(\beta)$ follows a β^3 law for small bending angles. This can be easily confirmed by expanding the a- and b-coordinates into Taylor series. From symmetry, each a_n is symmetric with respect to the bending angle, i.e. $a_{n(\beta)}=a_{n(-\beta)}$, and the a_n-expansions only include even powers of β. On the other hand the b_n are antisymmetric functions of β and their expansions only include odd powers of β:

$$a_{n(\beta)} = a_{n(0)} + \frac{1}{2!}\cdot a''_{n(0)}\cdot\beta^2+\dots,$$
$$b_{n(\beta)} = b'_{n(0)}\cdot\beta + \frac{1}{3!}\cdot b'''_{n(0)}\cdot\beta^3+\dots. \tag{51}$$

From the definition of I_{ab} in (46) and the constraint of zero internal angular moment (eq. (35)), which also holds at $\beta=0$

$$0=\sum_n m_n a_{n(0)}\cdot b'_{n(0)} \tag{52}$$

the off diagonal element I_{ab} indeed expands as

$$I_{ab(\beta)} = \sum_n m_n(a_{n(0)}\, b'''_{n(0)}/3! + a''_{n(0)}\, b'_{n(0)}/2!)\cdot\beta^3 + \dots\beta^5+\dots. \tag{53}$$

q.e.d.

With the small angle approximation $I_{ab}=0$ the classical zero field Hamiltonian reduces to the handy form:

$$H_0=\frac{1}{2I_{\beta\beta}}P_\beta^2+V_{(\beta)}+\frac{1}{2I_{aa}}P_a^2+\frac{1}{2I_{bb}}P_b^2+\frac{1}{2I_{cc}}P_c^2. \tag{54}$$

Since the moments of inertia depend on the bending angle, β, our classical Hamiltonian must be rearranged into "Podolsky-form" [32] prior to translation into quantum mechanics. Quite in general, a classical Hamiltonian formulated in curvilinear coordinates, q_k and the conjugate momenta P_k:

$$H_{\text{classical}}=\tfrac{1}{2}\sum_{ik} g_{ik}P_iP_k+V \tag{55}$$

translates to the Hamiltonian operator:

$$\hat H=\tfrac{1}{2}g^{1/4}\sum_{ik}\hat P_i\frac{g_{ik}}{g^{1/4}}\hat P_k\, g^{1/4}+V, \tag{56}$$

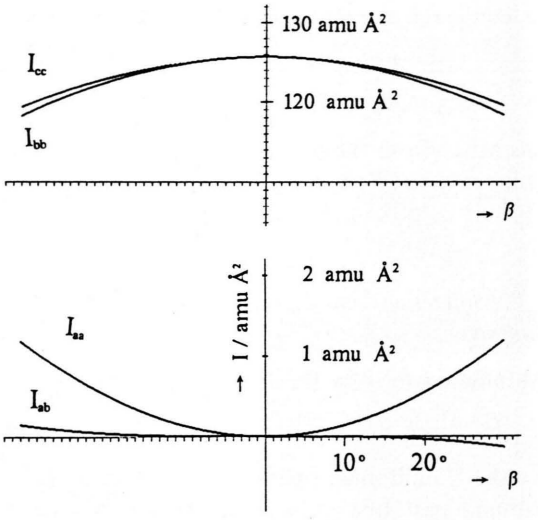

Fig. A.2. β-dependence of the elements of the moment of inertia tensor for $^{16}O=^{12}C=^{80}Se$ in the rigid bender approximation, i.e. with the bond distances fixed to their equilibrium values.

where g is the determinant of the matrix (g_{ik}). In our case

$$g=\det(\mathbf{I}^{-1})$$

is a function of β.

Since the rotational angular momentum operators $\hat P_g$ $(g=a,b,c)$ commute with their coefficients, the only complication which arises from this rearrangement is associated with the term involving $\hat P_\beta$:

$$\hat P_\beta\equiv\frac{\hbar}{i}\frac{\partial}{\partial\beta}. \tag{57}$$

If we retain only the leading term in the Taylor expansions of the moments of inertia with respect to β, we arrive at the following approximation to the zero field Hamiltonian:

$$\hat H_0=-\frac{\hbar^2}{2\cdot\sum m_n b'^2_{n(0)}}\frac{\partial^2}{\partial\beta^2} + \left\{V_{(\beta)}-\frac{\hbar^2}{8\cdot\sum m_n b'^2_{n(0)}\cdot\beta^2}\right\}+\frac{\hbar^2}{2I_{aa}}\hat J_a^2 + \frac{\hbar^2}{2I_{bb}}\hat J_b^2+\frac{\hbar^2}{2I_{cc}}\hat J_c^2=\hat H_{\text{vib, eff}}+\hat H_{\text{rot, eff}}. \tag{58}$$

In (58) we have written the angular momentum operators in terms of their dimensionless counterparts: $\hbar\hat J_g=\hat P_g$ $(g=a,b,c)$.

As compared to (54) there is an additional term:

$$-\frac{\hbar^2}{8\sum m_n b'^2_{n(0)}\cdot\beta^2}\,.$$

It has arisen from the rearrangement of the classical Hamiltonian to "Podolsky form", and it simulates a contribution to the potential energy.

8.4. Eigenfunctions and Eigenvalues of the Zero Field Hamiltonian

We now try to solve the eigenvalue problem:

$$\hat{H}_0\,\Psi = E\,\Psi\,. \tag{59}$$

Since the Hamiltonian operator consists of a purely vibrational part (first and second term in (58)) and an asymmetric top like contribution (third till fifth term in (58)) it appears reasonable to write the eigenfunctions as a product of an asymmetric top wave function, $\psi_{JK_aK_cM}(\varphi,\vartheta,\chi)$ and of a purely vibrational wave function, $\psi_v(\beta)$:

$$\Psi_{JK_aK_cMv}(\vartheta,\varphi,\chi,\beta)=\psi_{JK_aK_cM}(\vartheta,\varphi,\chi)\cdot\psi_v(\beta)\,. \tag{60}$$

Here ϑ, ψ, and χ are the three Eulerian angles which specify the instantaneous orientation of the molecular coordinate system with respect to the laboratory frame. Since the moments of inertia do not have fixed values as in the rigid rotor model, but are functions of the bending angle β, this "Ansatz" is not generally successful. However, for the low J states, which are of interest here, it helps. The reason for this can be traced back to the fact that the low J eigenfunctions of the asymmetric top which correspond to $J=1$ or 2 and $K_a=1$ are given by the symmetrized combinations of the symmetric top wave functions:

$$\Phi_{JK_aM}(\varphi,\vartheta,\chi)$$

such as

$$\frac{1}{\sqrt{2}}\left(\Phi_{J,K_a,M}(\vartheta,\varphi,\chi)\pm\Phi_{J,-K_a,M}(\vartheta,\varphi,\chi)\right)$$

irrespective of the values for the rotational constants (⇒Wang functions). These functions not only diagonalize the asymmetric rotor part of the Hamiltonian but also lead to integer expectation values for the squares of the angular momentum operators $\langle|\hat{J}_g^2|\rangle$. They are given in Table A.1 (cf. [24], Chapt. VII.2). To exploit this property we apply the Hamiltonian $\hat{H}_0$ to the product function defined in (60):

$$\hat{H}_0\psi_v\cdot\psi_{JK_aK_cM}\stackrel{?}{=}E\cdot\psi_v\cdot\psi_{JK_aK_cM}\,. \tag{61}$$

The question mark indicates that it is not yet perfectly clear at this stage whether such an identity will hold.

We now multiply from the left with the complex conjugate of $\psi_{JK_aK_cM}$ and integrate over the Eulerian angles. For the low J rotational wave functions of interest here, i.e. for ψ_{111M}, ψ_{110M}, ψ_{212M}, and ψ_{211}, and with the $\langle|\hat{J}_g^2|\rangle$ matrix elements compiled in Table A.1 we obtain:

$$\begin{aligned}E\psi_v(\beta)=&-\frac{\hbar^2}{2\sum m_n b'^2_n}\cdot\frac{\partial^2\psi_v(\beta)}{\partial\beta^2}\\&+\left(V(\beta)+\frac{\hbar^2}{2\sum m_n b'^2_n}\left[\langle|\hat{J}_a^2|\rangle-\tfrac{1}{4}\right]\cdot\beta^{-2}\right)\cdot\psi_v(\beta)\\&+\frac{\hbar^2}{2\sum m_n(a_n^2+a_n\,a''_n\,\beta^2)}\langle|\hat{J}_b^2|\rangle\,\psi_v(\beta)\\&+\frac{\hbar^2}{2\sum m_n(a_n^2+[a_n\,a''_n+b'^2_n]\,\beta^2)}\langle|\hat{J}_c^2|\rangle\,\psi_v(\beta)\,.\end{aligned} \tag{62}$$

Equation (62) corresponds to a vibrational Schrödinger equation with an effective potential energy which, through the expectation values $\langle|\hat{J}_g^2|\rangle$, depends on the specific rotational state. Especially $\langle|\hat{J}_a^2|\rangle$ generates an effective centrifugal potential similar to the "Podolsky correction" but larger in magnitude and with positive sign. Since (62) may be solved numerically by the Numerov-Cooley method, the product function in (61) with $\psi_v(\beta)$ chosen as the appropriate solution of (62) is indeed an exact eigenfunction of the zero field Hamiltonian as given in (58).

To gain some additional insight, we introduce several approximations, which will enable us to present analyt-

Table A.1. The low-J asymmetric top wave functions are given by linear combinations of symmetric top wavefunctions, $\Phi_{J,K_a,M}$, with coefficients which do not depend on the values of the rotational constants, A, B, and C. The Table gives the asymmetric top designations, linear combinations, energies in terms of the rotational constants and the expectation values of the squares of the angular momentum operators $\hat{J}_a$, $\hat{J}_b$, $\hat{J}_c$.

$J_{K_aK_c}$	$\Psi_{J,K_a,K_c,M}$	E_{J,K_a,K_c}	$\langle J_a^2\rangle$	$\langle J_b^2\rangle$	$\langle J_c^2\rangle$
1_{11}	$(\Phi_{1,1,M}+\Phi_{1,-1,M})/\sqrt{2}$	$A+C$	1	0	1
1_{10}	$(\Phi_{1,1,M}-\Phi_{1,-1,M})/\sqrt{2}$	$A+B$	1	1	0
2_{12}	$(\Phi_{2,1,M}+\Phi_{2,-1,M})/\sqrt{2}$	$A+B+4C$	1	1	4
2_{11}	$(\Phi_{2,1,M}-\Phi_{2,-1,M})/\sqrt{2}$	$A+4B+C$	1	4	1

ical solutions to the effective vibrational Schrödinger equation. We introduce the harmonic oscillator approximation for the bending potential $V(\beta)$: $V(\beta) = \frac{1}{2} k \beta^2$ and we also neglect the slight β-dependence in the moments of inertia I_{bb} and I_{cc}. With these approximations (62) further simplifies to

$$\tilde{E}\psi_v(\beta) = -\frac{\hbar^2}{2\sum m_n b_n'^2} \cdot \frac{\partial^2 \psi_v(\beta)}{\partial \beta^2} + \left(\frac{1}{2} \cdot k \cdot \beta^2 + \frac{\hbar^2}{2\sum m_n b_n'^2} \cdot \frac{3}{4} \cdot \beta^{-2}\right) \cdot \psi_v(\beta), \tag{63}$$

where $\tilde{E}$ is the shorthand for

$$\tilde{E} = E - \frac{\hbar^2}{2\sum m_n a_n^2}\left(\langle|\hat{J}_b^2|\rangle + \langle|\hat{J}_c^2|\rangle\right). \tag{64}$$

By scaling of the bending angle, β and the energy, $\tilde{E}$, as:

$$\beta = c_\beta \cdot x, \quad \tilde{E} = c_E \cdot \tilde{\varepsilon} \tag{65}$$

this equation may be transformed to a standard form, applicable to all triatomic benders:

$$-\frac{\partial^2 \psi(x)}{\partial x^2} + [x^2 + \tfrac{3}{4} x^{-2}]\,\psi(x) = \tilde{\varepsilon}\psi(x). \tag{66}$$

To this end the scaling factors have to be chosen as

$$c_\beta = \left(\frac{\hbar^2}{\sum m_n b_n'^2} \frac{1}{k}\right)^{1/4}, \quad c_E = \frac{1}{2}\left(\frac{\hbar^2}{\sum m_n b_n'^2} k\right)^{1/2}. \tag{67}$$

Equations (62) or (63) may be regarded as the Schrödinger equations of the rigid bender in an effective potential which not only includes the true potential function $V_{(\beta)}$ in (62) – it corresponds to x^2 in (66) – but also a "centrifugal potential" x^{-2} in (66), and the Podolsky-correction", $-1/4 \cdot x^{-2}$ in (66), which let the effective potential go infinite with β or $x \to 0$. This centrifugal contribution very effectively prevents the molecule from swinging through its linear equilibrium configuration.

To derive the analytical solutions of (66) we write the solutions, $\psi(x)$, as a product of a Gaussian, $e^{-x^2/2}$, and a second function, $f(x)$, just as in the treatment of the standard harmonic oscillator.

$$\psi(x) = e^{-x^2/2} f(x). \tag{68}$$

Insertion of (68) into (66) leads to the following second order differential equation for $f(x)$:

$$-f'' + 2x f' + \frac{a}{x^2} f = (\tilde{\varepsilon} - 1) f. \tag{69}$$

By using the general constant "a" rather than the special value, $a = 3/4$, we generalize to a whole family of effective Schrödinger equations, which can all be solved by the same method.

We then write the solution as a polynomial expansion:

$$f(x) = x^r \sum_{n=0} c_n x^l. \tag{70}$$

Insertion into (69) and comparison of the coefficients of equal powers of x leads to

$$[r(r-1) - a]\, c_0 = 0 \tag{71}$$

or

$$r = \tfrac{1}{2} \pm \sqrt{a + \tfrac{1}{4}}. \tag{72}$$

Further it leads to the recursion

$$c_{n+2} = \frac{\tilde{\varepsilon} - 1 - 2r - 2n}{a - (r+n+2)(r+n+1)}. \tag{73}$$

(A similar pair of relations holds for the odd indices, but it does not carry any new information.)

Since $\psi^2(x)$ corresponds to a probability density, we are only interested in those solutions for which the integral

$$\int_{x=0}^{+\infty} \psi^2(x)\, dx$$

has a finite value.

This specifies the r-value in (72) to the one with the positive sign of the square root. It also leads to the requirement that the sequence of the c_l-coefficients should come to an end at some maximum value of the index n. Otherwise $f(x)$ would go infinite essentially as $e^{+(x^2)}$. To this end the nominator in the recursion (73) must hit zero at the appropriate n-value, n_{max}, and this defines the sequence of the eigenvalues, $\tilde{\varepsilon}$, as:

$$\tilde{\varepsilon}_{n_{max}} = 2r + 1 + 2n_{max}. \tag{74}$$

We note that since the index n proceeds in steps of 2, the spacing of the eigenvalues is 4, and this *irrespective* of the value of the constant "a" in the effective potential function. Thus in (66) all potential functions $V(x) = x^2 + a/x^2$ lead to the same constant spacing between adjacent eigenvalues, i.e. to $\Delta\tilde{\varepsilon} = 4$.

In our case, i.e. with the value $a = 3/4$, the three lowest eigenvalues and eigenfunctions of (66) are:

$$\begin{aligned} \tilde{\varepsilon} &= 4; \quad \psi(x) = N_4 x^{3/2} e^{-x^2/2}, \\ \tilde{\varepsilon} &= 8; \quad \psi(x) = N_8 x^{3/2}(1 - x^2/2)\, e^{-x^2/2}, \\ \tilde{\varepsilon} &= 12; \quad \psi(x) = N_{12} x^{3/2}(1 - x^2 + x^4/6)\, e^{-x^2/2}. \end{aligned} \tag{75}$$

Here N_4, N_8, N_{12} are the appropriate normalization factors. From the analytical solutions for the small angle Schrödinger equation one can calculate the corresponding expectation values of any power of x (or β). Such expectation values are needed for the comparison of measured molecular parameters with their theoretical expressions. In our context one may think of the paramagnetic susceptibilities or of the nuclear contribution to the molecular g-tensor. The availability of analytical expressions at least in these case of the small angle approximation is definitely helpful if one wants to get a feeling for the accuracy of numerical results such as obtained for instance by the Numerov-Cooley method. Actually, at present we do not see a way around the numerical approach to solve the original Schrödinger equation if the "small angle" approximation is dropped.

In Fig. A.3 we show the squared solution, $\psi^2(x)$, for the lowest vibrational state in the x-notation. The scaling factor $c_\beta = 0.128$ rad $\simeq 7.35°$ (see (67)) was calculated from the numerical value for the sum $\sum m_n b'^2_{n(0)} = 4.421$ amu Å/rad^2 and from the observed bending frequency $\nu_2 \simeq 464$ cm^{-1} [23] within the harmonic oscillator approximation for $V(x)$. Clearly, from this probability density in the ($K_a = 1, \upsilon_{\text{bending}} = 0$)-state the molecule may be looked at as a slightly bent asymmetric top with a bending angle on the order of ten degrees.

In the following section we treat the field dependent terms in the Hamiltonian given by (49) as perturbations to the zero field case.

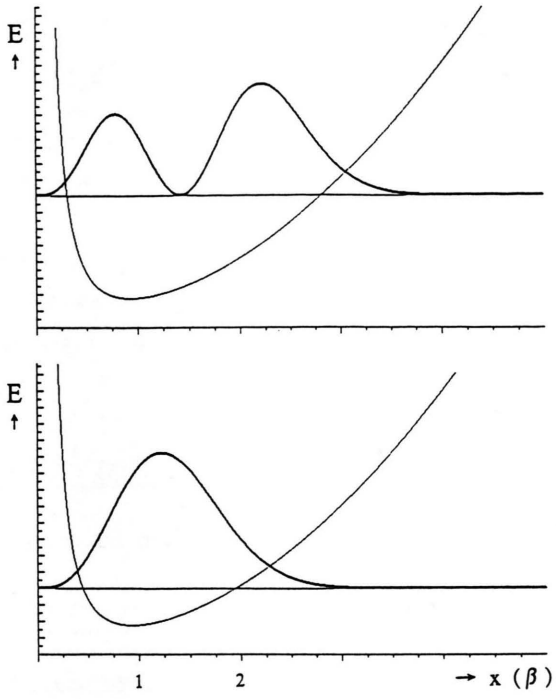

Fig. A.3. Probability density $\Psi^2(x)$ in the two lowest bending states with one quantum of angular momentum along the a-axis (top). For the conversion between the bending angle in degrees and the reduced bending coordinate x compare Eqs. (65) and (67) of the text.

8.5. Perturbation Treatment of the Zeeman Contribution

8.5.1. First and Second Order Perturbation Treatment of the Field Dependent Contributions in the Hamiltonian

In the following we will account for the field dependent parts in the Hamiltonian eq. (49) by first and second order perturbation theory. The second line in (49) is linear in the magnetic field. It leads to contributions which are associated with the molecular g-tensor elements in the effective energy expression used to analyse the Zeeman splittings (compare (10)). The third line in (49) is quadratic in H_Z. So in principle it will lead to contributions which are associated with the molecular susceptibility tensor. The fourth line is again linear in the magnetic field, but, as indicated already, we will treat it as if it were a Stark effect contribution.

Quite in general, if expressed in frequency units, the field dependent matrix elements fall into the MHz range, while the matrix elements due to the zero field Hamiltonian fall into the GHz range (and above). Thus only Zeeman matrix elements which are diagonal in the eigenfunction basis of the zero field Hamiltonian and from the off diagonal elements only those which connect the closely spaced K_a-doublet levels need to be considered here. From the four group (or asymmetric rotor group) symmetry properties (cf. Chapt. VII in [23]) of the angular momentum operators, $\hat{J}_g$, and of the direction cosines, $\cos(gZ)$, on the one hand and of the asymmetric top wave functions on the other hand the following results are obtained:

The only rotational operators which lead to diagonal matrix elements are the products $\cos(gZ)\hat{J}_g$, $\hat{J}_g \cos(gZ)$, $\hat{J}_g^2$, and $\cos^2(gZ)$ ($g = a, b, c$). The only off diagonal elements which may connect the closely spaced K_a-doublets arise from the direction cosine $\cos(aZ)$ in $\boldsymbol{\mu} \cdot \boldsymbol{E}_{\text{Lorentz}}$.

If we then drop all other parts in the Hamiltonian eq. (49) as practically irrelevant, the first and second order perturbations to be accounted for reduce to the following contributions.

First order contributions:

$$\langle \hat{H}_{\text{Zeeman}} \rangle = -\frac{\hbar}{4c} \left[\langle \Psi_v(\beta) | \frac{\sum q_n b_n(\beta)^2}{\sum m_n b_n(\beta)^2} | \Psi_v(\beta) \rangle \cdot \langle \Psi_{JK_aK_cM} | \cos aZ \hat{J}_a + \hat{J}_a \cos aZ | \Psi_{JK_aK_cM} \rangle \right]$$

$$+ \langle \Psi_v(\beta) | \frac{\sum q_n a_n(\beta)^2}{\sum m_n a_n(\beta)^2} | \Psi_v(\beta) \rangle \cdot \langle \Psi_{JK_aK_cM} | \cos bZ \hat{J}_b + \hat{J}_b \cos bZ | \Psi_{JK_aK_cM} \rangle$$

$$+ \left[\langle \Psi_v(\beta) | \frac{\sum q_n (a_n(\beta)^2 + b_n(\beta)^2)}{\sum m_n (a_n(\beta)^2 + b_n(\beta)^2)} | \Psi_v(\beta) \rangle \cdot \langle \Psi_{JK_aK_cM} | \cos cZ \hat{J}_c + \hat{J}_c \cos cZ | \Psi_{JK_aK_cM} \rangle \right]. \quad (76)$$

These contributions are linear in the magnetic field strength and contribute to the g-tensor elements in the phenomenological Hamiltonian. Terms involving $\hat{P}_\beta$ do not contribute since they are connected with $\cos cZ$ and $\langle \Psi_{JK_aK_cM} | \cos cZ | \Psi_{JK_aK_cM} \rangle = 0$. Also $\langle \Psi_v(\beta) | \hat{P}_\beta | \Psi_v(\beta) \rangle$ is zero.

In principle there are also first order contributions, which are quadratic in the magnetic field strength. These contributions arise from the expectation values of $\frac{1}{2} \mathbf{Z}^t \cdot \mathbf{I}^{-1} \cdot \mathbf{Z}$ and include for instance the term:

$$\frac{1}{4c} H_Z^2 \langle \Psi_v(\beta) | \frac{(\sum q_n (a_n^2 + b_n^2))^2}{\sum m_n (a_n^2 + b_n^2)} | \Psi_v(\beta) \rangle \langle \Psi_{JK_aK_cM} | \cos^2 cZ | \Psi_{JK_aK_cM} \rangle .$$

In the phenomenological Hamiltonian they correspond to contributions to the magnetic susceptibility tensor (cf. Eq. (IV,55,j) in [14]). Apart from the fact that they involve effective atomic charges, q_n, rather than nuclear charges, $Z_n |e|$, they have the form of nuclear contributions to the magnetic susceptibility tensor and are numerically negligible (cf. p. 173 through p. 176 in [14]). Thus, within our atomic point charge model, we cannot account for the susceptibilities. We will come back to this point below.

Second order contributions

The only significant second order perturbation contributions arise from the "translational Stark effect", i.e. from $-\boldsymbol{\mu}_a \cdot \boldsymbol{E}_{\text{Lorentz}}$, since the direction cosine $\cos aX$ leads to non-vanishing asymmetric top matrix elements between the closely spaced K_a-doublets. The modification of the Zeeman multiplet patterns associated with the translational Stark effect has been discussed already in the main section of this contribution. In the final section we discuss the electronic contributions to the g- and ξ-tensor elements.

8.5.2. The Electronic Contributions to the g- and ξ-Tensor Elements

For the explicit inclusion of the electrons we can draw heavily on the theory developed in [14]. The only difference with respect to the rigid nuclear frame model treated there is the inclusion of one internal nuclear degree of freedom, the bending motion. As a result the inverse of the generalized moment of inertia tensor there (Eq. (IV.37) in [14]) and the "Zeeman vector" $\boldsymbol{\Gamma}$ (Eq. (IV.22) in [14]) have to be modified as follows.

The 3×3 submatrix corresponding to the inverse of the molecular moment of inertia tensor (fourth to sixth row and column, resp., of Eq. (IV.37) in [14]) has to be replaced by the 4×4 submatrix given in (45).

One additional element, $\Gamma_\beta = Z_\beta$, has to be inserted into the "Zeeman vector" $\boldsymbol{\Gamma}$ after Γ_c with Z_β essentially defined as in (45), but with our atomic point charges q_n replaced by the charges of the corresponding nuclei, $Z_n |e|$.

This essentially leads to the same classical Hamiltonian as derived in [14] but with Eq. (IV.55.e) there replaced by our zero field Hamiltonian eq. (50) and with an extra field dependent term:

$$\frac{1}{2} (P_\beta - Z_\beta) \frac{1}{I_{\beta\beta}} (P_\beta - Z_\beta) .$$

If the second order perturbation treatment within the vibronic states is then carried out along the same lines as described in the Appendix A III of [14], with our bending angle playing the role of the vibrational coordinate there, one indeed arrives at the conclusion that the vibrational ground state expectation values for the asymmetric top expressions for the g- and ξ-tensor elements are appropriate approximations to the theoretical expressions for the g- and ξ-tensor elements in our effective energy expression (10).

Acknowledgements

We would like to thank Prof. H. Willner, Hannover, for preparing the sample, and Dr. J. Demaison, Lille, for suggesting the present study. We would also like to thank Prof. D. G. Lister, Messina, who critically corrected our English. Financial support by Deutsche Forschungsgemeinschaft and Fonds der Chemischen Industrie is gratefully acknowledged.

[1] L. Engelbrecht and D. H. Sutter, Z. Naturforsch. **33a,** 1525 (1978).
[2] W. Hüttner and K. Morgenstern, Z. Naturforsch. **25a,** 547 (1970).
[3] W. Hüttner, K. Bodenseh, and P. Nowicki, Mol. Phys. **35,** 729 (1978).
[4] B. J. Howard and R. E. Moss, Mol. Phys. **20,** 147 (1971).
[5] R. E. Moss and A. J. Perry, Mol. Phys. **25,** 1121 (1973).
[6] R. L. Shoemaker and W. H. Flygare, Chem. Phys. Lett. **6,** 576 (1970).
[7] H. Bürger, M. Litz, H. Willner, M. Le Guennec, G. W. Wlodarczak, and J. Demaison, J. Molec. Spectrosc. **146,** 220 (1991).
[8] O. Böttcher, B. Kleibömer, and D. H. Sutter, Ber. Bunsenges. Phys. Chem. **93,** 207 (1989).
[9] J. C. McGurk, T. G. Schmalz, and W. H. Flygare, Adv. Chem. Phys. **XXV,** 1 (1974).
[10] H. Dreizler, Mol. Phys. **59,** 1 (1986).
[11] O. Böttcher and D. H. Sutter, Z. Naturforsch. **43a,** 47 (1988).
[12] J. Haeckel and H. Mäder, Z. Naturforsch. **43a,** 203 (1988).
[13] H. Bürger, J. Molec. Spectrosc. **140,** 270 (1991).
[14] D. H. Sutter and W. H. Flygare, The Molecular Zeeman Effect. Topics in Curr. Chem. **63,** 91–196 (1976).
[15] Compare [14] Appendix A III.
[16] G. Wlodarczak and W. Stahl, private communication of the spin rotation coupling constant.
[17] M. Le Guennec, These, Lille 1992, p. 107, Table IV.
[18] F. Holland, A. Klesing, D. H. Sutter, and U. Fleischer, J. Molec. Spectrosc. **161,** 44 (1993).
[19] M. J. Frisch, M. J. Head-Gordon, O. W. Trucks, J. B. Foresman, H. B. Schlegel, H. B. Schlegel, K. Raghavachari, M. Robb, J. S. Binkley, C. Gonzales, D. J. De Frees, D. J. Fox, R. A. Whiteside, R. Seeger, C. F. Melius, J. Baker, R. L. Martin, L. R. Kahn, J. J. P. Stewart, S. Topiol, and J. A. Pople, GAUSSIAN, Inc., Pittsburgh, PA, 1990.
[20] P. J. Hay and W. R. Wadt, J. Chem. Phys. **82,** 284 (1985).
[21] C. H. Townes, G. C. Dousmanis, A. D. White, and R. F. Schwarz, Discussions Faraday Soc. **19,** 56 (1955).
[22] T. Wentik, M. W. P. Strandberg, and R. Hilger, Bull. Amer. Phys. Soc. **23,** 18 (1948).
[23] H. Bürger, M. Litz, H. Willner, M. Le Guennec, G. Wlodarczak, and J. Demaison, J. Molec. Spectrosc. **146,** 220 (1991).
[24] Walter Gordy and Robert L. Cook, Microwave Molecular Spectra, 3rd ed., John Wiley & Sons, New York 1984, Chapt VII.
[25] B. Numerov, Publs. Observatoire Central Astrophys. Russ. **2,** 188 (1933).
[26] J. W. Cooley, Math. Comp. **15,** 363 (1961).
[27] J. M. L. Reinartz, W. L. Meerts, and A. Dymanus, Chem. Phys. Lett. **16,** 576 (1972).
[28] Walter Weizel, Lehrbuch der Theoretischen Physik, Springer Verlag, Heidelberg 1955, Chapt. A.II, § 6.
[29] J. T. Hougen, P. R. Bunker, and J. W. C. Johns, J. Molec. Spectrosc. **34,** 136 (1970).
[30] L. D. Landau and E. M. Lifshitz, Lehrbuch der Theoretischen Physik, Vol. I, Mechanik, Chapt. I, § 2. Akademie-Verlag, Berlin 1967.
[31] E. Bright Wilson Jr., J. C. Decius, and P. C. Cross, Molecular Vibrations, Chapts. 11-2 through 11-5. McGraw-Hill, New York 1955.
[32] E. C. Kemble, The Fundamental Principles of Quantum Mechanics, Chapt. VII, Sect. 35. Dover Publications, New York 1958.